

TREND: Transferability based Robust ENsemble Design

Deepak Ravikumar*, Sangamesh Kodge*, Isha Garg*
and Kaushik Roy, *Fellow, IEEE*
(* Equal contributors)

Abstract—Deep Learning models hold state-of-the-art performance in many fields, but their vulnerability to adversarial examples poses a threat to their ubiquitous deployment in practical settings. Additionally, adversarial inputs generated on one classifier have been shown to transfer to other classifiers trained on similar data, which makes the attacks possible even if the model parameters are not revealed to the adversary. This property of transferability has not yet been systematically studied, leading to a gap in our understanding of robustness of neural networks to adversarial inputs. In this work, we study the effect of network architecture, initialization, input, weight and activation quantization on transferability. Our experiments reveal that transferability is significantly hampered by input quantization and architectural mismatch between source and target, is unaffected by initialization and is architecture-dependent for both weight and activation quantization. To quantify transferability, we propose a simple metric, which is a function of the attack strength. We demonstrate the utility of the proposed metric in designing a methodology to build ensembles with improved adversarial robustness. Finally, we show that an ensemble consisting of carefully chosen input quantized networks achieves better adversarial robustness than would otherwise be possible with a single network.

I. INTRODUCTION

Deep learning has become state-of-the-art for many machine learning tasks over the past few years. Deep neural networks (DNNs) have achieved human level performance in image recognition [1], [2]. They have also been used for speech recognition [3] and natural language processing [4]. However, recent research [5], [6], [7] has shown the existence of small perturbations which when added to the input can cause DNNs to misclassify the input. These adversarial perturbations are imperceptible to the human eye and are crafted with the specific intent of fooling deep neural networks into misclassifying the images. The existence of adversarial inputs has led to a considerable knowledge gap in the explainability of deep neural nets, which limits their use in safety critical applications such as malware detection [8] or autonomous driving systems [9].

The generation of adversarial inputs usually requires access to the target network (the network to be attacked) in the form of network weights or logits. However, in most practical scenarios, the adversary does not have access to the internal parameters, but is able to observe the output of the network for a given input [10]. In such cases, previous works [11], [12], [13] have shown that the adversary can train a substitute network by

generating synthetic data using the outputs or the logits of the target network. Such query based attacks, often labeled as black-box attacks, are successful because of the transferability of adversarial perturbations: attacks crafted to fool one network often fool another network trained on similar data.

In this paper, with the motive of understanding the transferability of adversarial images between networks, we systematically study how transferability is affected by network architecture, network initialization, input, weight and activation quantization. To account for these factors, we propose a metric of transferability as a function of the attack strength. Additionally, we show that understanding transferability aids in building robust ensembles of DNNs.

The key contributions of this work are summarised as follows:

- We explore the effect of network initialization, model architecture, quantization of input, weight and activation on transferability of adversarial images from one DNN to another. We also make empirical suggestions on the most effective model to use, both from the point of view of an adversary and defender. These experiments were performed on various small and large datasets, attacked using PGD [14]. Additionally, we study the effect of attack strength (ϵ) on transferability;
- We fit the number of images that transfer from one model to another as the Cumulative Distribution Function (CDF) of an exponential distribution. Using this, we propose a simple metric of transferability as a function of attack strength (ϵ), that can be estimated with as few as 4 empirical datapoints and generalizes to a continuum of epsilons;
- We devise an effective method for adversarially attacking an ensemble of DNNs;
- We outline a methodology, TREND (Transferability based Robust ENsemble Design), which uses the proposed transferability metric to build an ensemble with higher robustness than would otherwise be possible with a single DNN.

II. RELATED WORK

Attack Methodologies. Many methods have been proposed for generating adversarial inputs. Some of the popular attacks in literature are Fast Gradient Sign Method (FGSM) [6], a single step attack; Basic Iterative Method (BIM) [7], a multi-step iterative attack; Carlini Wagner Attack (CW) [15], an

The authors are with the School of Electrical and Computer Engineering, Purdue University, West Lafayette, IN 47906 USA (e-mail: {dravikum, skodge, gargi, kaushik}@purdue.edu).

optimization based attack; and Projected Gradient Descent (PGD)[14], an iterative version of FGSM with a random start point within an ϵ bound around the clean image. There are numerous other attacks like Jacobian-based Saliency Map Attack (JSMA) [16], DeepFool [17], and Elastic-Net Attacks (EADAttack) [18]. However, PGD is currently the strongest known attack, and therefore, we study transferability under this attack. We utilize Back-Propagation through Differential Approximation (BPDA) [19] style gradient back-propagation to allow gradients to propagate through any non-differentiable functions such as input or activation quantization, wherever needed.

Transferability. The ability of adversarial perturbations generated on one model to successfully fool other models was first observed in [5] and subsequently in [6]. It has been shown that transferability is not unique to deep learning, but exists across various machine learning classifiers [20]. They show transferability across DNNs, k-Nearest Neighbors, Decision Trees, Support Vector Machines and Logistic Regression. Such transfer attacks can be implemented successfully in both targeted or non-targeted scenarios [21]. Moreover, the transferability of adversarial examples is hypothesized to occur due to the alignment of the decision boundaries across various models [21]. The adversarial examples are shown to span a contiguous subspace of high dimensionality (≈ 25) [22]. The authors find that a significant factor of this subspace is shared between two models, which they attribute to the closeness of the decision boundaries learnt by the models. However, authors of [23] argue that the transfer is asymmetric and hence, cannot be explained completely by closely aligned decision boundaries.

Ensembles. Ensemble methods leverage the averaging effects of multiple models to make a final prediction. Model averaging methods include bagging [24] and boosting [25], [26]. We consider one of the simplest approaches to make decisions: the majority voting strategy. Ensembles are used as a tool to reduce variance in classifiers [27]. However, we utilize them to gain adversarial robustness without significantly degrading the performance on clean images. Recent research [28], [29], [30] has focused on developing defense strategies using ensembles. However, it has been shown [31] that ensembles are not immune to adversarial attacks. In this paper, we take a deeper look at the link between transferability and the adversarial accuracy of ensembles, first suggested in [31]. We show that careful selection of individual DNNs that make up the ensemble can improve the overall robustness of the ensemble.

III. EXPERIMENTAL SETUP

In this section, we perform experiments to study how network initialization, network architecture, input, weight and activation quantization affect transferability. We study the effect of these factors independently on CIFAR-10, CIFAR-100 [32] and ImageNet [33] datasets.

All the models in the paper were trained using the stochastic gradient descent optimizer with a momentum of 0.9 and weight decay of 5×10^{-4} . The models were trained for 250 epochs on the ImageNet dataset and 350 epochs on CIFAR-10 and

CIFAR100 datasets. Initial learning rate was set to 10^{-2} and it was scaled down by a factor of 10 at 60% and 80% completion using a learning rate scheduler. At the end of each epoch the model was evaluated on the validation set and the model weights that achieved the best validation accuracy was saved. The model weights that achieved the best validation accuracy was used to evaluate the network performance on the test set and its accuracy was reported. Table I shows the training, validation and test set sizes for each dataset used.

Preliminaries. Let the input to a DNN be represented by x , its true class be denoted by t , and the neural net classifier be represented by the function $f(x)$. Then $x' = x + \delta$, where $-\epsilon \leq \delta \leq \epsilon$, is said to be an adversarial input to the network if $f(x) = t$ and $f(x') \neq t$. Here, ϵ represents the maximum allowed perturbation with respect to a distance metric, generally L_∞ , L_2 or L_0 norm. The norm is given by $\|x\|_p = (\sum_{i=1}^n |x_i|^p)^{(1/p)}$ where $p = 0$ for L_0 , $p = 2$ for L_2 and so on. Images are considered adversarial if the changes are imperceptible to humans but fool the network. To limit the allowable change, bounds are set on the perturbation norm to maintain imperceptibility. We consider the L_∞ distance between the original and the perturbed image as the measure of change.

Transferability. We study transferability between models by generating adversarial images on the source model and evaluating them on the target model. To generate the adversarial images, we run PGD for 40 iterations with an ϵ of $8/255$ and step size of 0.01, unless otherwise mentioned. An image is considered to transfer to the target model if the clean image is classified correctly by both the source and the target model and the adversarial image is misclassified by both the models. To decouple the effect of accuracy of the source and target models, we run our experiments on a subset of 1000 images that are correctly classified by all the models under consideration.

Confusion Matrices. We present results as a confusion matrix which represents the number of images transferred as a fraction of the subset size (1000). Hence a value of 0.14 translates to 140 adversarial images transferred from source to target, out of the 1000 generated on the source. The deeper the color of the cell, the higher the transferability between the corresponding source and target model. The normalized transferability number can also be viewed as the factor with which the adversarial accuracy of the black box model is expected to decrease. The rows and columns represent the effect of changing the target model or the source model, respectively. An adversary performing black box attacks has control over only the source model and would want to choose a model with the highest row average, in order to successfully attack a range of target models. Similarly, a defender controls only the target model and would want to choose the model with the lowest column average, in order to have the lowest transferability across any chosen source model. The averages are therefore shown alongside the corresponding rows and columns. The confusion matrices for CIFAR-10, CIFAR-100 and ImageNet are shown in Blue, Green and Orange respectively.

TABLE I: Training, Validation and Test set sizes for the datasets used

Dataset	Train Set Size	Validation Set Size	Test Set Size
CIFAR-10	45,000 (90%)	5,000 (10%)	10,000
CIFAR-100	45,000 (90%)	5,000 (10%)	10,000
ImageNet	1,249,137 (97.5%)	32,029 (2.5%)	50,000

TABLE II: Baseline model accuracies in % and the number of images transferred from source to target on CIFAR-10 and CIFAR-100 datasets for differently seeded models.

Architecture	CIFAR-10					CIFAR-100				
	Seed	1	2	3	4		1	2	3	4
ResNet18	Acc	91.85	92.04	91.91	92.53	Acc	72.56	72.80	72.61	72.48
	Trans.	1000	509	534	566	Trans.	1000	707	688	648
VGG11	Acc	87.21	88.20	87.57	87.41	Acc	55.5	56.87	56.56	55.80
	Trans.	1000	717	760	709	Trans.	1000	638	682	637
VGG11 BN	Acc	87.66	87.76	87.97	88.11	Acc	60.07	60.29	60.22	60.40
	Trans.	1000	695	697	655	Trans.	1000	468	446	436

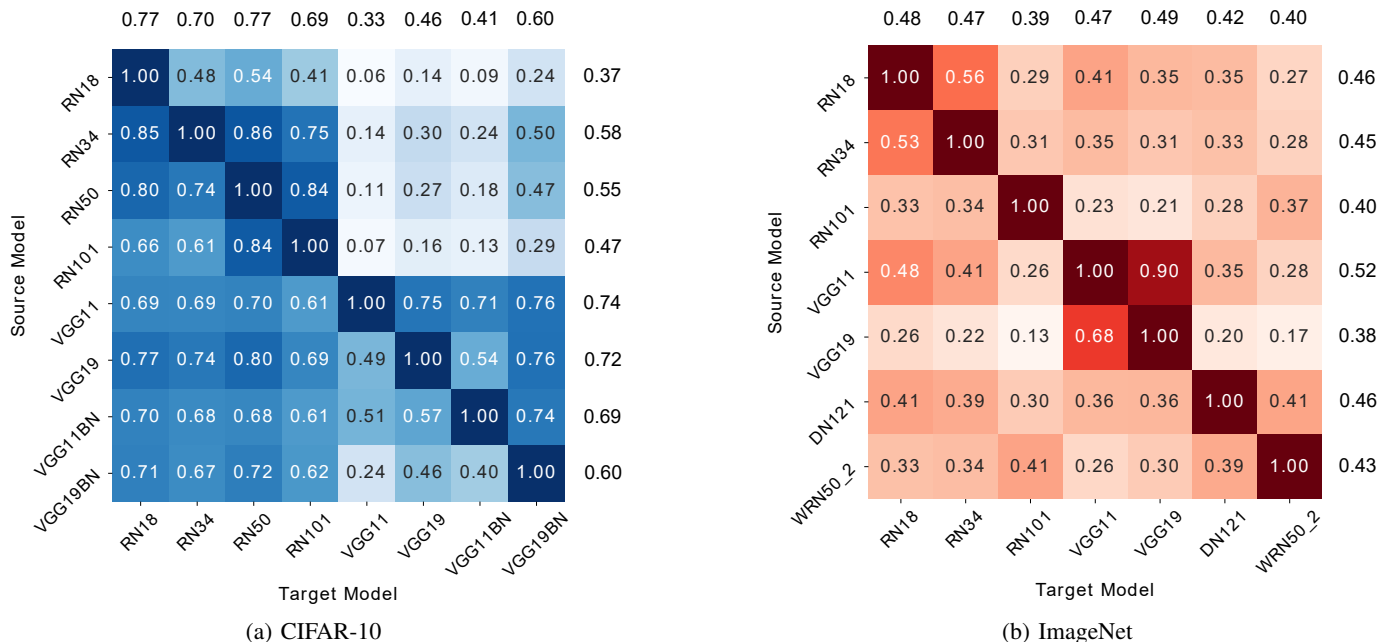


Fig. 1: Number of adversarial images transferred from source to target for various architectures.

IV. TRANSFERABILITY ANALYSIS

A. Network Initialization

The gradient descent algorithm is known to be sensitive to initialization [34]. Different parameter initializations lead training to converge to different solutions [35]. We investigate the effect of initialization by training four models with different random initial seeds. In this study we consider ResNet18 [36], VGG11 and the batch normalized version of VGG11 (VGG11 BN) [37] architectures.

Table II shows the baseline accuracies and the number of adversarial images transferred from the source to the target model under PGD attack. The source model for each architecture was initialized with ‘Seed 1’. We highlight in blue the case where the source and the target models are identical and the number of images transferred represents the

number of adversarial images generated on that particular model. We observe that the number of images transferred does not radically change across different seeds, for all the models. **This suggests that initialization does not play a significant role in transferability.** Table II also seems to imply that architecture is an important consideration for transferability. We investigate this in the next subsection.

B. Architecture

We study the effect of architecture on transferability by analyzing cross model transfer of adversarial images between ResNet18 (RN18), ResNet34 (RN34), ResNet101 (RN101), VGG11, VGG19, VGG11BN, VGG19BN, DenseNet121 (DN121) [38] and WideResNet50_2 (WRN50_2) [39]. Figure 1 shows the number of adversarial images transferred from

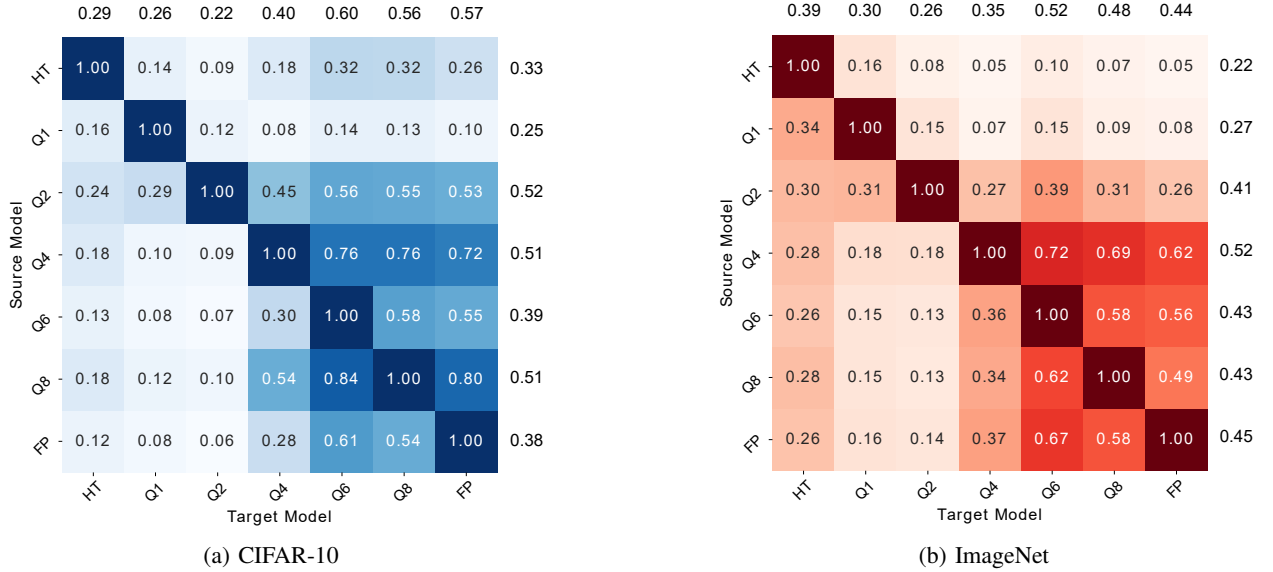


Fig. 2: Number of adversarial images transferred from source to target for input quantized models.

source to target for various architectures on CIFAR-10 and ImageNet (see Appendix II for CIFAR-100 results).

Figure 1a can be interpreted by analyzing the 4 quadrants, with each quadrant representing a family of source or target model architectures (ResNet or VGG variants). The top right quadrant of Figure 1a is lighter than the bottom left quadrant. This implies that adversarial images generated on VGG are more transferable to ResNets than the other way around. The results for CIFAR-100 follow the same trend and are shown Appendix II. Surprisingly, we find that the matrices are considerably asymmetric. These findings reveal that transferability is not commutative. Another empirical observation is that the left half of Figure 1a is the darkest, implying that ResNets are more susceptible to transfer attacks. This susceptibility has been leveraged to build better transfer attacks [40] and is attributed to skip connections [40]. These trends also hold for ImageNet. From Figure 1, we observe that the column averages for ResNet18, ResNet34, VGG11 and VGG19 are among the highest. The high column average for VGG networks can be attributed to intra-family transferability, with just two numbers boosting up the column average. Hence, **VGG models are better source models for the adversary** because the row averages for VGG networks are consistently high across various datasets and provides the highest chances for successful black-box attacks. **ResNets are easier targets and should therefore be avoided by defenders**, as they consistently show very high column averages across various datasets.

C. Quantization

Recent research [29], [30], [41] suggests that quantization has potential to provide robustness against adversarial images. We expect these trends to be applicable to transferability as well. Therefore, we study how input, weight and activation quantization affect transferability. For all experiments hence-

forth, our base model is ResNet18. Results for VGG11 as the base model are presented in Appendix III and IV.

1) *Input Quantization*: Input quantization as the name suggests, quantizes the input to the network. We analyze various input bit widths ranging from 8-bits down to 1-bit per channel, per pixel for both the source and the target models.

We quantize a minibatch of images using the following formula,

$$I_{quant} = \left\lfloor \frac{I - i_{min}}{b} \right\rfloor b + \left(\frac{1}{2}b + i_{min} \right) \quad (1)$$

where I_{quant} is the quantized minibatch of images, b is the bin width defined as

$$b = \frac{i_{max} - i_{min}}{2^n} \quad (2)$$

where n is the bit-width used for input quantization, i_{min} is the minimum and i_{max} is the maximum value of the minibatch I . This scheme is similar to the one suggested by [40], the difference being, we normalize the input before quantization. The inputs were normalized using the mean and standard deviation of the training dataset. We also consider the non-linear quantization scheme of halftoning mentioned in [42]. The quantized models are represented by "Q_ibit-width_i", halftone by "HT" and "FP" refers to the full precision network. We use BPDA [19] based gradient backpropagation through the quantization scheme. The baseline accuracies of models trained on different input bit-widths are presented in the Appendix I. From Figures 2a and 2b (see Appendix III for CIFAR100 results), we see that low bit width input quantized models (HT, Q1 and Q2) have very low transferability. Additionally, transferability of input quantized models is highly asymmetric. It is far easier to transfer from Q2 to various models than it is to transfer to Q2. This is also true for Q4 and HT, though to a lesser extent. To further understand the effect of input quantization, we visualize the decision boundaries of the network. The basis (i.e. x and y axes) of the visualization

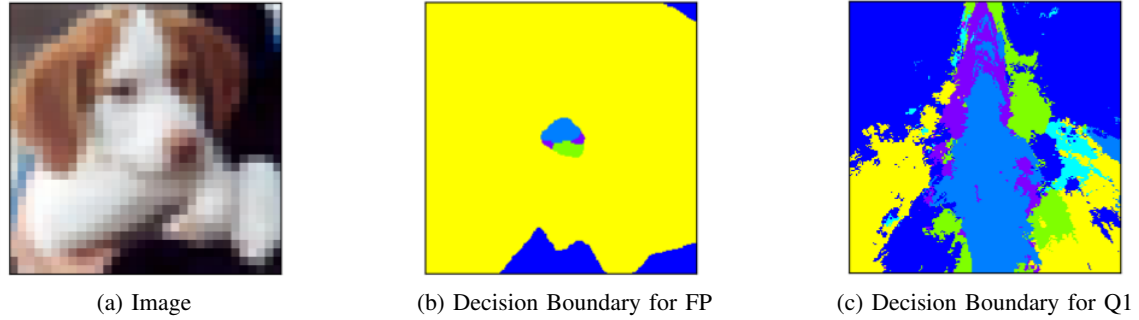


Fig. 3: Decision boundaries around image 3a the of a full precision and 1-bit quantized input model

shown in Figure 3 were chosen to be the normalized adversarial gradient vector obtained from PGD (x-axis) and a random vector orthogonal to the former. Using these two vectors as the basis, the input space was traversed and the corresponding classes represented with different colors. The centers of Figures 3b and 3c represent 3a in the input space. **We observe that input quantization increases the distance to the decision boundary in most directions**, however, transfer attacks still successfully find adversarial examples.

This leads us to conclude that **low bit width input quantization significantly reduces the success of transfer attacks**. For instance, quantizing the inputs of CIFAR-10 from FP to Q1 improves adversarial accuracy by $\sim 9\%$ between Q1 and FP. **Input quantized models with bit width greater than 2 make better source models for adversaries**. This is because these models have high row averages (see Figure 2) which results in the highest chance for a successful black-box transfer attack. **Input quantized models with bit widths 1, 2 or HT are more robust to transfer attacks, and hence make better target models for the defenders**. This is clear from the low column averages (see Figure 2) for these models across various datasets, provide the best chance of defense.

2) *Weight and Activation Quantization*: In this subsection, we study how quantizing the network parameters and activations affect the number of images transferred. Figure 4 shows the transferability among ResNet18 models with different weight and activation bit precisions for CIFAR-10 (see Appendix IV for CIFAR-100 results). The weight quantized models are represented by "W_ibit-width_i", activation quantized models are represented by "A_ibit-width_i" and "FP" represents 32-bit full precision model. Results for VGG weight and activation quantized models are available in Appendix IV. We find that the trends for activation and weight quantization are highly dataset and architecture dependent. It is difficult to make generic recommendations for the adversary or the defender. We show the confusion matrices for different datasets and architectures in Appendix IV, and the relevant ones can be consulted when making a decision.

D. Transferability Metric

The previous subsections show that transferability is affected by a multitude of factors. In this subsection, we analyze the variation of transferability with respect to the attack strength ϵ . We plot the number of images that transfer between different

source-target models, referred to as $f_{st}(\epsilon)$, for 20 different values of ϵ in Fig. 5. We observe that these curves cross one another and therefore the trends of transferability across models cannot be generalized from the observations at a single ϵ . However, we are interested in plotting this curve with the fewest possible measurements, such that it would have good predictive power over a range of ϵ values. To do this, we note that each plot visually resembles the CDF of an exponential distribution. The same is true for the number of images generated on a model, denoted by f_{ss} . Hence, we characterize both functions in the following form:

$$f_{st}(\epsilon) = a(1 - e^{b\epsilon}) \quad (3)$$

$$f_{ss}(\epsilon) = a'(1 - e^{b'\epsilon}) \quad (4)$$

where a , a' , b and b' are the parameters for fitting the data, obtained experimentally. We find the parameters of the equation using a few datapoints. Figure 5 shows the empirical curve obtained using 20 points, and the predicted curve, fit using 4 points. We observe that they align well and we get a 5% Root Mean Square Error (RMSE) for the fit. Table III shows the standard error (RMSE) for the fit used to calculate the transferability metric.

TABLE III: Transferability Metric Fit Confidence for CIFAR10

Source Model	Target Model	Standard Error Train (RMSE)	Standard Error Test (RMSE)
VGG11	VGG11	114.41	505.23
RESNET18	RESNET18	38.67	480.64
VGG11	RESNET18	661.34	516.65
RESNET18	VGG11	44.58	46.72
VGG11 Seed1	VGG11 Seed2	529.92	405.56
RESNET18 Seed1	RESNET18 Seed2	358.37	248.17
FP	Q1	12.63	47.11
Q1	FP	352.34	423.61

Armed with these observations, we propose a simple but effective transferability metric that quantifies transferability as a function of attack strength ϵ . In the previous subsection we capture transferability as a ratio of the number of images that transfer to the target to the number of images that were generated at the source. Equivalently our generative model of transferability normalizes f_{st} by f_{ss} and gives us the transferability metric, TM:

$$TM(\epsilon) = \frac{f_{st}(\epsilon)}{f_{ss}(\epsilon)} \quad (5)$$

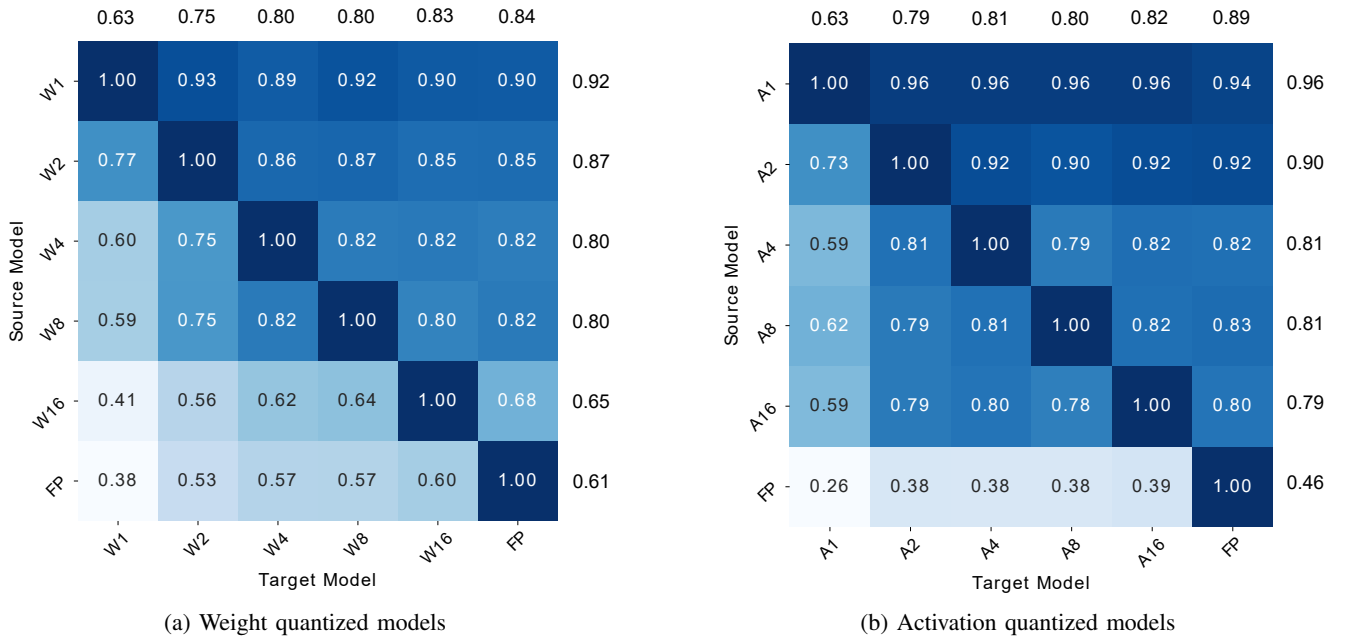


Fig. 4: Number of adversarial images transferred from source to target on CIFAR-10 dataset.

The transferability metric is a number between $[0, 1]$ and represents a quantitative measure of the transferability between a given pair of models. The constants in both equations capture the effects of dataset, architecture, input quantization etc. and can be estimated with a few datapoints. For example, we use 4 datapoints to estimate the constants for various quantizations for CIFAR-10. The predicted values are shown in Figure 6 and the experimentally obtained values are shown in Figure 2a. The close match between Figure 6 and 2a shows the effectiveness of the proposed transferability metric in predicting adversarial input transferability. The average difference between the predicted and actual values is 0.055 or 5.5% for CIFAR-10 dataset on ResNet18 base model. Results for CIFAR-100 are presented in Appendix V and reflect a good match between the predicted and simulated values.

V. ASSEMBLING THE RIGHT ENSEMBLE

Recent research [28], [29], [30] suggests that ensembles provide robustness against adversarial attacks. The robustness of the ensemble, or the lack thereof, is hypothesized to arise from the property of transferability [31]. Since images are transferable to different models, an image meant to fool one network will fool a majority of the networks in the ensemble and therefore, the whole ensemble. We delve deeper into this hypothesis by constructing ensembles with models that have varying transferability between them, as captured by the transferability metric proposed in Subsection IV-D. We expect ensembles with models that have a high transferability metric (averaged by exchanging the source and target) between them to be less robust, as an image that fools one model will transfer well and fool the ensemble. We can assemble ensembles of any order by choosing pairs of models with low transferability metric among them, resulting in an ensemble with improved robustness. In the subsequent sections, we go into the details of how to effectively attack and design ensembles.

A. Attacking an Ensemble

Optimization based attacks like PGD use the gradient of the input with respect to the loss function to decide the direction of change. However, the choice of gradient direction is not easily apparent for an ensemble. The simplest way is to average the gradient [43] from each model. This is referred to as the **Gradient Average** attack. However, the gradients from different models in an ensemble tend to cancel each other out, especially when the attack strength is low. Hence, we devise more effective ways to generate the gradient direction for an ensemble. The first method, which we call **Sign All** chooses only those gradient directions where all the individual models' gradient directions align. The second method, or **Sign Average**, calculates the gradient direction for the ensemble by averaging the sign of the gradients from each model.

Sign All. In this approach gradient direction for the ensemble as a whole is given by

$$\text{sgn}(G_{ensemble}) = \begin{cases} x & x = y : x, y \in S_i, S_j \forall i \neq j; i, j \in [1, N] \\ 0 & \text{otherwise} \end{cases} \quad (6)$$

where sgn is the signum or sign function, $S_i = \text{sgn}(G_i)$ is the sign of the gradient from individual model i and N is the number of models in the ensemble. Equation 6 translates to choosing only those gradient directions where all the individual model's gradient directions are in agreement.

Sign Average. In this approach, the gradient direction for the ensemble is calculated by averaging the sign of the gradients from each model.

$$\text{sgn}(G_{ensemble}) = \frac{1}{N} \sum_{m=1}^N \text{sgn}(G_m) \quad (7)$$

where sgn is the sign function, G_m is the gradient from an individual model m and N is the number of models in the ensemble.

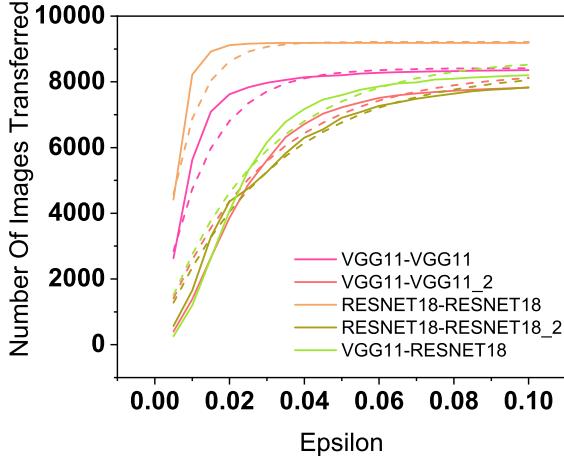


Fig. 5: Predicted (dotted) and actual (solid) number of images transferred vs attack strength ϵ for CIFAR-10 from (source-target). Here `_2` refers to differently seeded model.

Source Model	HT	Q1	Q2	Q4	Q6	Q8	FP
HT	1.00	0.15	0.16	0.32	0.43	0.42	0.38
Q1	0.26	1.00	0.23	0.25	0.29	0.28	0.28
Q2	0.35	0.28	1.00	0.60	0.65	0.67	0.63
Q4	0.26	0.12	0.17	1.00	0.72	0.73	0.71
Q6	0.19	0.10	0.12	0.43	1.00	0.64	0.60
Q8	0.25	0.12	0.17	0.61	0.77	1.00	0.76
FP	0.19	0.10	0.12	0.42	0.62	0.61	1.00
Target Model	HT	Q1	Q2	Q4	Q6	Q8	FP

Fig. 6: Transferability metric for various models on CIFAR-10 at ϵ of 8/255, obtained from equation 5, fit using 4 datapoints. The empirical counterpart is found in Fig 8b

Sign Average is significantly more effective than Gradient Average because it acts only on the signs of the individual gradient and thus avoids confusion because of the magnitudes. Figure 7 shows the results for the Gradient Average, Sign All and Sign Average attacks and it can be seen that Sign Average performs significantly better than other approaches. We use this attack for testing our ensembles in the subsequent sections.

B. Robust Ensemble Design

In this subsection, we utilize the transferability metric introduced in Subsection IV-D to put forth a methodology TREND, to build an ensemble with improved robustness. The ensembles predicts a class using majority voting. In case of conflict (i.e. no majority vote), one of the models is chosen

at random and its output is considered as the ensemble’s prediction. The hypothesis that high transferability between models in an ensemble results in reduced adversarial robustness was first suggested in [31]. We leverage this idea and build an ensemble with improved robustness by choosing models with low transferability. To identify these models, we consider a list of all pairs of individual models under consideration and calculate the transferability metric for each pair. To account for asymmetry, we average the two numbers obtained by interchanging source and target. From this list, we choose a desired number of models with the lowest transferability metric. Figure 6 shows the transferability metric between various input quantized configurations of ResNet18 trained on CIFAR-10. The ensembles built using this method were evaluated using the attacks described in Subsection V-A. From Figure 7 we see that the ensemble of FP-Q1-Q2 consistently outperforms other ensembles with respect to adversarial robustness. This trend was expected from Figure 6, which predicts that Q1, Q2 and HT have the lowest average transferability metric. The trend holds for different datasets, as shown in Appendix VI. The Appendix VI also details various ensemble combinations and their adversarial accuracies under attack, and the trends expected from the transferability metric hold. Ensemble, FP-Q1-Q2, designed using TREND is seen to be $\approx 25\%$ more robust than Q1, Q2 or FP individually. The improved robustness is seen as an increase in L_∞ perturbation needed to fool such ensembles when compared to ensembles consisting of models with high transferability as seen in Figure 7. The parameters used for PGD were the same as in Section IV, except the number of iterations was reduced to 20 to shorten the simulation time.

VI. DISCUSSION AND CONCLUSION

TREND is a methodology to systematically design an ensemble with improved adversarial robustness. In this paper we analyze the effect of DNN initialization, architecture, and input, weight and activation quantization on transferability. Our analysis suggests that initialization has no significant effect on transferability, that the ResNet architecture is more susceptible to transfer attacks than the other architectures considered and quantizing the inputs significantly reduces transferability. The reduction in transferability holds true only when the inputs are quantized to low bit widths (one and two bits). Additionally, our experiments reveal that the effect of weight and activation quantization is highly dependent on the dataset. We also observe that transferability is asymmetric. If adversarial images transfer well from source to target, the vice versa need not necessarily be true. Additionally, wherever applicable, we offer guidelines for the construction of defense and attack models based on the transferability trends observed. To account for the effect of attack strength, epsilon, we propose a simple transferability metric that can be estimated with very few measurements and generalizes to a continuum of epsilons. The constants that fit the distribution can be estimated with as little as 4 experimental datapoints, and capture the dependencies on all considered factors such as architecture, quantization and initialization. We employ the transferability metric to

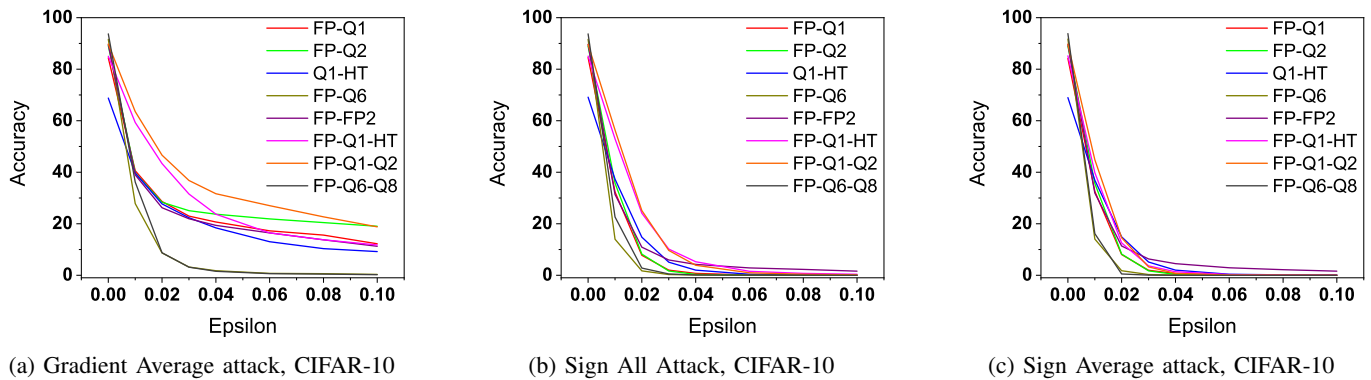


Fig. 7: Accuracies in % of various ensembles as a function of attack strength ϵ when using Gradient Average, Sign All and Sign Average attack. From the plots, we see that models with low transferability form more robust ensembles.

design robust ensembles that require stronger attack strength compared to the constituting models for a similar accuracy degradation. Our results clarify that the adversarial robustness of an ensemble is indeed determined by how transferable an adversarial image is among the models in the ensemble. Using the predicted values from the transferability metric, we are able to construct ensembles with improved robustness.

ACKNOWLEDGEMENT

This work was supported in part by the Center for Brain Inspired Computing (C-BRIC), one of the six centers in JUMP, a Semiconductor Research Corporation (SRC) program sponsored by DARPA, by the Semiconductor Research Corporation, the National Science Foundation, Intel Corporation, the DoD Vannevar Bush Fellowship, and by the U.S. Army Research Laboratory and the U.K. Ministry of Defence under Agreement Number W911NF-16-3-0001.

REFERENCES

- [1] A. Krizhevsky, I. Sutskever, and G. Hinton, “Imagenet classification with deep convolutional neural networks,” *Advances in Neural Information Processing Systems (NeurIPS)*, vol. 25, 01 2012.
- [2] Y. LeCun, Y. Bengio, and G. Hinton, “Deep learning,” *Nature*, vol. 521, no. 7553, pp. 436–444, 2015. [Online]. Available: <https://doi.org/10.1038/nature14539>
- [3] G. Hinton, L. Deng, D. Yu, G. E. Dahl, A. Mohamed, N. Jaitly, A. Senior, V. Vanhoucke, P. Nguyen, T. N. Sainath, and B. Kingsbury, “Deep neural networks for acoustic modeling in speech recognition: The shared views of four research groups,” *IEEE Signal Processing Magazine*, vol. 29, no. 6, pp. 82–97, 2012.
- [4] D. Andor, C. Alberti, D. Weiss, A. Severyn, A. Presta, K. Ganchev, S. Petrov, and M. Collins, “Globally normalized transition-based neural networks,” *Proceedings of the 54th Annual Meeting of the Association for Computational Linguistics (Volume 1: Long Papers)*, 2016. [Online]. Available: <http://dx.doi.org/10.18653/v1/P16-1231>
- [5] J. Bruna, C. Szegedy, I. Sutskever, I. Goodfellow, W. Zaremba, R. Fergus, and D. Erhan, “Intriguing properties of neural networks,” *International Conference on Learning Representation (ICLR), Poster*, 2014.
- [6] I. J. Goodfellow, J. Shlens, and C. Szegedy, “Explaining and harnessing adversarial examples,” *International Conference on Learning Representation (ICLR), Poster*, 2015.
- [7] A. Kurakin, I. Goodfellow, and S. Bengio, “Adversarial examples in the physical world,” *International Conference on Learning Representation (ICLR), Workshop Track*, 2017. [Online]. Available: <https://openreview.net/forum?id=S1OufnIlx>
- [8] G. E. Dahl, J. W. Stokes, L. Deng, and D. Yu, “Large-scale malware classification using random projections and neural networks,” *IEEE International Conference on Acoustics, Speech and Signal Processing*, pp. 3422–3426, 2013.
- [9] N. Papernot, P. McDaniel, I. Goodfellow, S. Jha, Z. B. Celik, and A. Swami, “Practical black-box attacks against machine learning,” *Proceedings of ACM on Asia conference on computer and communications security*, pp. 506–519, 2017.
- [10] A. N. Bhagoji, W. He, B. Li, and D. Song, “Practical black-box attacks on deep neural networks using efficient query mechanisms,” *European Conference on Computer Vision (ECCV)*, pp. 158–174, 2018.
- [11] Y. Guo, Z. Yan, and C. Zhang, “Subspace attack: Exploiting promising subspaces for query-efficient black-box attacks,” *Advances in Neural Information Processing Systems (NeurIPS)*, vol. 32, pp. 3820–3829, 2019.
- [12] P.-Y. Chen, H. Zhang, Y. Sharma, J. Yi, and C.-J. Hsieh, “Zoo: Zeroth order optimization based black-box attacks to deep neural networks without training substitute models,” *Proceedings of the 10th ACM Workshop on Artificial Intelligence and Security*, pp. 15–26, 2017.
- [13] N. Narodytska and S. P. Kasiviswanathan, “Simple black-box adversarial attacks on deep neural networks,” *Proceedings of the IEEE Conference on Computer Vision and Pattern Recognition Workshops (CVPR)*, pp. 6–14, 2017.
- [14] A. Madry, A. Makelov, L. Schmidt, D. Tsipras, and A. Vladu, “Towards deep learning models resistant to adversarial attacks,” *International Conference on Learning Representation (ICLR)*, 2017.
- [15] N. Carlini and D. Wagner, “Towards evaluating the robustness of neural networks,” *IEEE Symposium on Security and Privacy*, pp. 39–57, 2017.
- [16] N. Papernot, P. McDaniel, S. Jha, M. Fredrikson, Z. B. Celik, and A. Swami, “The limitations of deep learning in adversarial settings,” *IEEE European Symposium on Security and Privacy*, 2016.
- [17] S.-M. Moosavi-Dezfooli, A. Fawzi, and P. Frossard, “Deepfool: a simple and accurate method to fool deep neural networks,” *Conference on Computer Vision and Pattern Recognition (CVPR)*, 2016.
- [18] P.-Y. Chen, Y. Sharma, H. Zhang, J. Yi, and C.-J. Hsieh, “Ead: Elastic-net attacks to deep neural networks via adversarial examples,” *Association for The Advancement of Artificial Intelligence (AAAI)*, 2018.
- [19] A. Athalye, N. Carlini, and D. A. Wagner, “Obfuscated gradients give a false sense of security: Circumventing defenses to adversarial examples,” in *International Conference on Learning Representations (ICLR)*, 2018, pp. 274–283. [Online]. Available: <http://proceedings.mlr.press/v80/athalye18a.html>
- [20] N. Papernot, P. D. McDaniel, and I. J. Goodfellow, “Transferability in machine learning: from phenomena to black-box attacks using adversarial samples,” *Computer Research Repository (CoRR)*, vol. abs/1605.07277, 2016.
- [21] Y. Liu, X. Chen, C. Liu, and D. X. Song, “Delving into transferable adversarial examples and black-box attacks,” *International Conference on Learning Representation (ICLR)*, 2017. [Online]. Available: <https://openreview.net/forum?id=Sys6GJqxl>
- [22] F. Tramèr, N. Papernot, I. Goodfellow, D. Boneh, and P. McDaniel, “The space of transferable adversarial examples,” *Computer Research Repository (CoRR)*, 2017.
- [23] L. Wu, Z. Zhu, C. Tai *et al.*, “Understanding and enhancing the

- transferability of adversarial examples,” *arXiv preprint arXiv:1802.09707*, 2018.
- [24] L. Breiman, “Bagging predictors,” *Machine Learning*, vol. 24, no. 2, pp. 123–140, Aug 1996. [Online]. Available: <https://doi.org/10.1023/A:1018054314350>
- [25] Y. Freund and R. E. Schapire, “Game theory, on-line prediction and boosting,” in *Proceedings of the Ninth Annual Conference on Computational Learning Theory*, ser. COLT 96. New York, NY, USA: Association for Computing Machinery, 1996, p. 325332. [Online]. Available: <https://doi.org/10.1145/238061.238163>
- [26] —, “Experiments with a new boosting algorithm,” in *Proceedings of the Thirteenth International Conference on International Conference on Machine Learning*, ser. ICML96. San Francisco, CA, USA: Morgan Kaufmann Publishers Inc., 1996, p. 148156.
- [27] U. Naftaly, N. Intrator, and D. Horn, “Optimal ensemble averaging of neural networks,” *Network: Computation in Neural Systems*, vol. 8, 07 1999.
- [28] M. Abbasi and C. Gagné, “Robustness to adversarial examples through an ensemble of specialists,” *ArXiv*, vol. abs/1702.06856, 2017.
- [29] W. Xu, D. Evans, and Y. Qi, “Feature squeezing: Detecting adversarial examples in deep neural networks,” *Proceedings 2018 Network and Distributed System Security Symposium*, 2018. [Online]. Available: <http://dx.doi.org/10.14722/ndss.2018.23198>
- [30] S. Sen, B. Ravindran, and A. Raghunathan, “Empir: Ensembles of mixed precision deep networks for increased robustness against adversarial attacks,” in *International Conference on Learning Representations (ICLR)*, 2020. [Online]. Available: <https://openreview.net/forum?id=HJem3yHKwH>
- [31] W. He, J. Wei, X. Chen, N. Carlini, and D. Song, “Adversarial example defense: Ensembles of weak defenses are not strong,” in *11th USENIX Workshop on Offensive Technologies, WOOT 2017, Vancouver, BC, Canada, August 14-15, 2017*, W. Enck and C. Mulliner, Eds. USENIX Association, 2017. [Online]. Available: <https://www.usenix.org/conference/woot17/workshop-program/presentation/he>
- [32] A. Krizhevsky, G. Hinton *et al.*, “Learning multiple layers of features from tiny images,” 2009.
- [33] J. Deng, W. Dong, R. Socher, L.-J. Li, K. Li, and L. Fei-Fei, “ImageNet: A Large-Scale Hierarchical Image Database,” *Conference on Computer Vision and Pattern Recognition (CVPR)*, 2009.
- [34] J. F. Kolen and J. B. Pollack, “Back propagation is sensitive to initial conditions,” *Advances in Neural Information Processing Systems (NeurIPS)*, vol. 3, pp. 860–867, 1991. [Online]. Available: <http://papers.nips.cc/paper/395-back-propagation-is-sensitive-to-initial-conditions.pdf>
- [35] I. Sutskever, J. Martens, G. Dahl, and G. Hinton, “On the importance of initialization and momentum in deep learning,” *International conference on machine learning (ICML)*, pp. 1139–1147, 2013.
- [36] K. He, X. Zhang, S. Ren, and J. Sun, “Deep residual learning for image recognition,” *Conference on Computer Vision and Pattern Recognition (CVPR)*, pp. 770–778, 2016.
- [37] K. Simonyan and A. Zisserman, “Very deep convolutional networks for large-scale image recognition,” *International Conference on Learning Representations (ICLR)*, 2015.
- [38] G. Huang, Z. Liu, L. Van Der Maaten, and K. Q. Weinberger, “Densely connected convolutional networks,” *Conference on Computer Vision and Pattern Recognition (CVPR)*, pp. 2261–2269, 2017.
- [39] S. Zagoruyko and N. Komodakis, “Wide residual networks,” *British Machine Vision Conference (BMVC)*, 2016.
- [40] D. Wu, Y. Wang, S.-T. Xia, J. Bailey, and X. Ma, “Skip connections matter: On the transferability of adversarial examples generated with resnets,” in *International Conference on Learning Representations*, 2020. [Online]. Available: <https://openreview.net/forum?id=BJIRs34Fvr>
- [41] P. Panda, I. Chakraborty, and K. Roy, “Discretization based solutions for secure machine learning against adversarial attacks,” *IEEE Access*, vol. 7, pp. 70 157–70 168, 2019.
- [42] S. Kodge, H. Chaudhary, and M. Sharad, “Low power image acquisition scheme using on-pixel event driven halftoning,” *2017 IEEE Computer Society Annual Symposium on VLSI (ISVLSI)*, pp. 260–265, 2017.
- [43] F. Tramer, N. Carlini, W. Brendel, and A. Madry, “On adaptive attacks to adversarial example defenses,” 2020.

APPENDIX

I. BASELINE ACCURACIES

The baseline accuracies of the quantized models on different datasets with base architecture ResNet18 and VGG11 are shown in Table IV and V respectively. Baselines accuracies for different architecture are presented in Table VI

TABLE IV: Baseline model accuracies for quantized inputs, weight and activations on CIFAR-10, CIFAR-100 and ImageNet with ResNet18 as baseline

Quantization	CIFAR-10	CIFAR-100	ImageNet
FP	91.85%	72.56%	55.73%
Q8	92.52%	72.79%	55.63%
Q6	91.36%	72.15%	55.39%
Q4	91.42%	71.32%	55.09%
Q2	85.83%	62.21%	50.12%
Q1	75.80%	47.92%	40.27%
HT	84.44%	55.98%	46.95%
W16	91.85 %	71.91%	-
W8	92.15%	72.63%	-
W4	91.45%	66.63%	-
W2	90.87%	63.2%	-
W1	90.13%	56.77%	-
A16	90.20%	65.95%	-
A8	90.17%	66.62%	-
A4	90.10%	67.01%	-
A2	89.36%	61.49%	-
A1	87.08%	57.73%	-

TABLE V: Baseline model accuracies for quantized inputs, weight and activations on CIFAR-10 and CIFAR-100 with VGG11 as baseline

Quantization	CIFAR-10	CIFAR-100
FP	87.21%	55.50%
Q8	87.74%	56.58%
Q6	87.61%	55.24%
Q4	87.10%	54.50%
Q2	82.58%	50.44%
Q1	74.10%	37.88%
HT	80.74%	46.27%
W16	88.16%	56.58%
W8	88.16%	55.24%
W4	87.75%	54.50%
W2	86.82%	50.44%
A16	88.45%	57.33%
A8	88.15%	57.63%
A4	87.63%	41.12%
A2	87.00%	57.71%
A1	74.74%	32.76%

II. ARCHITECTURE ANALYSIS

Figure 8a shows the number of adversarial images transferred from source to target for various architectures on CIFAR-100. Figure 8a can be interpreted by analyzing the 4 quadrants, with each quadrant representing a family of source or target model architectures (ResNet or VGG variants). The top right quadrant of Figure 8a is lighter than the bottom left quadrant. This implies that adversarial images generated on VGG are more transferable to ResNets than the other way around.

TABLE VI: Baseline model accuracies for different architectures on CIFAR-10, CIFAR-100 and ImageNet with ResNet18 as baseline

Quantization	CIFAR-10	CIFAR-100	ImageNet
RN18	91.85%	72.56%	69.76%
RN34	92.16%	73.40%	73.31%
RN50	91.53%	69.37%	-
RN101	92.83%	70.47%	77.37%
VGG11	87.21%	55.5%	69.02%
VGG19	88.29%	59.07%	72.38%
VGG11BN	87.66%	60.07%	-
VGG19BN	89.83%	62.10%	-
DN121	-	-	74.43%
WRN50_2	-	-	78.47%

III. INPUT QUANTIZATION

Figure 8b, Figure 9a and Figure 9b show the variation in transferability due input quantization on CIFAR-10 and CIFAR-100 with ResNet and VGG as the base models.

IV. WEIGHT AND ACTIVATION QUANTIZATION

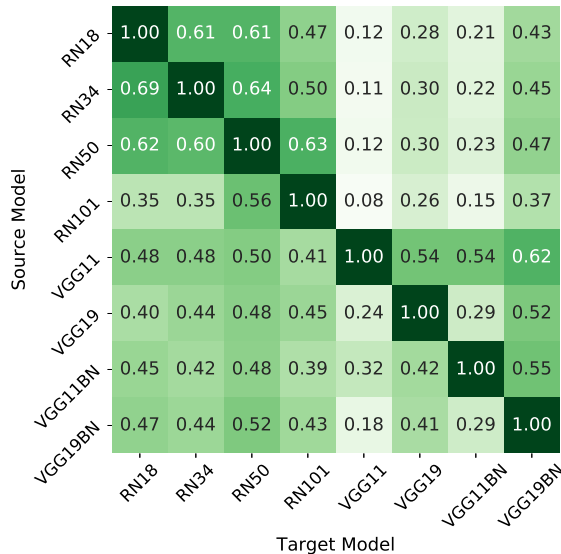
Figure 10 shows the confusion matrices for activation and weight quantized models on CIFAR-100. Figure 11 shows the confusion matrices for activation and weight quantized VGG11 models on CIFAR-10. Figure 10a and Figure 10b use ResNet18 as their base models while Figure 10c and Figure 10d use VGG11 as their base model.

V. TM FOR DIFFERENT DATASETS

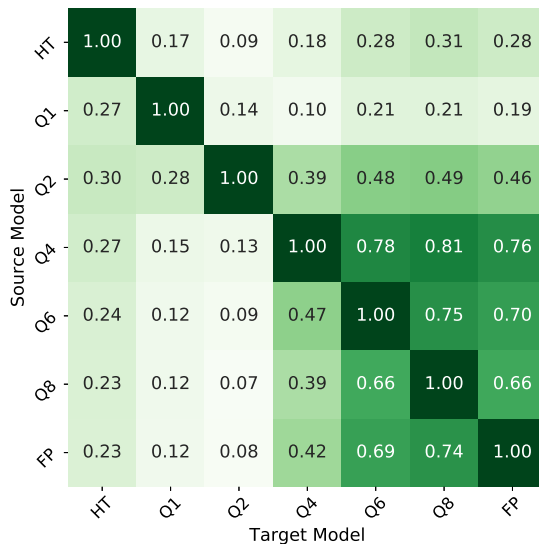
Figure 12 presents the observed transferability metric for input quantized networks and Figure 13 shows the error in the predicted and observed values of transferability metric for CIFAR10 and CIFAR100 datasets. Figure 14 shows the observed transferability metric and the prediction error for input quantized networks.

VI. RESULTS FOR DIFFERENT ENSEMBLES

From Figure 13 and 14b we observe that Q1, Q2 and HT are robust models for CIFAR-10, CIFAR-100 and ImageNet datasets. The result for ensemble on CIFAR-10 and CIFAR-100 under different attacks are shown in Figure 15.

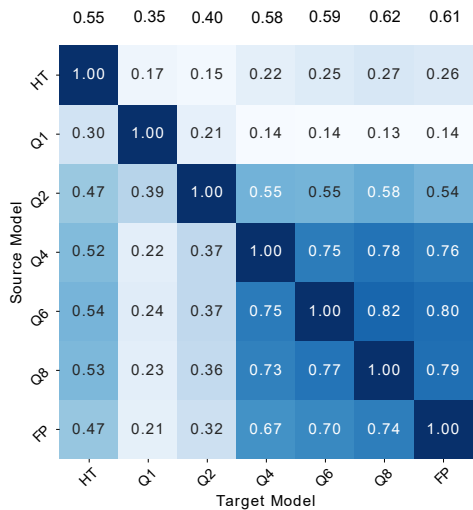


(a) Architecture analysis

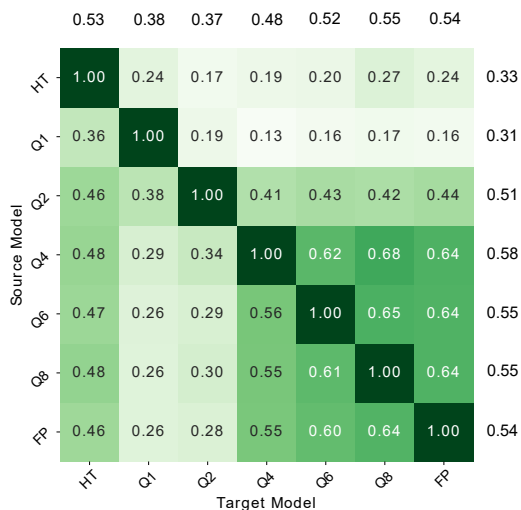


(b) Input quantization analysis, ResNet18 base model

Fig. 8: Number of adversarial images transferred from source to target on CIFAR-100 dataset with Subset size of 1000

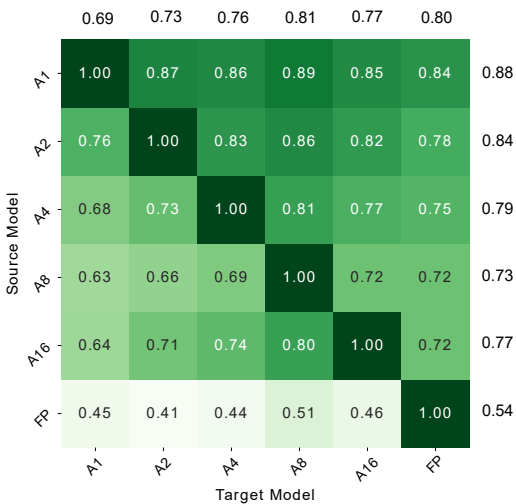


(a) Input quantization analysis, VGG11 base model, CIFAR-10

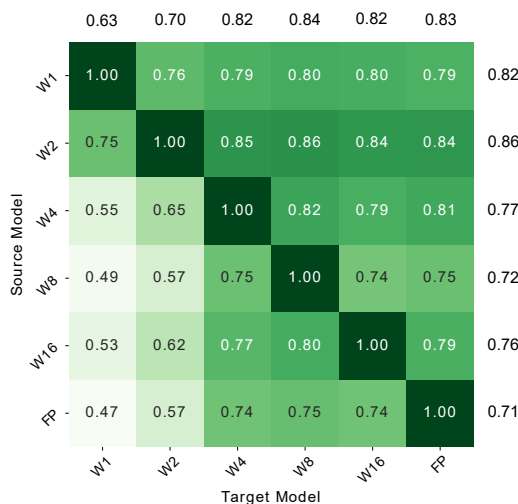


(b) Input quantization analysis, VGG11 base model, CIFAR-100

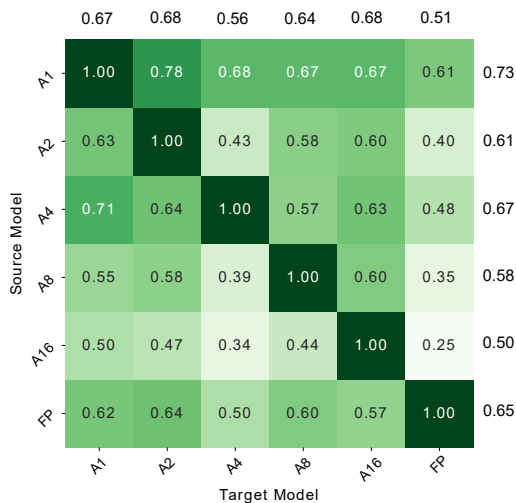
Fig. 9: Number of adversarial images transferred from source to target on CIFAR-10 and CIFAR-100 dataset



(a) Activation quantized ResNet18 models



(b) Weight quantized ResNet18 models

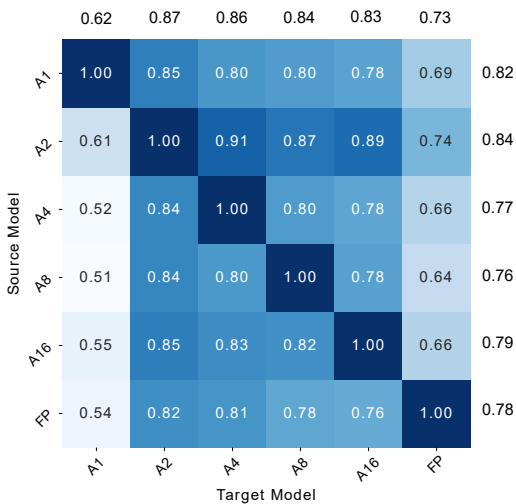


(c) Activation quantized VGG11 models

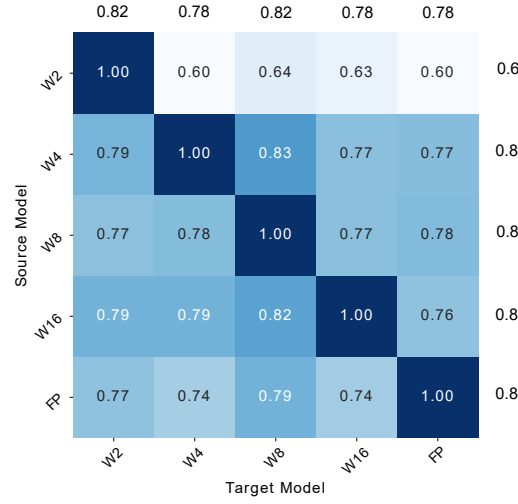


(d) Weight quantized VGG11 models

Fig. 10: Number of adversarial images transferred from source to target on CIFAR-100 dataset (with Subset size of 3000)

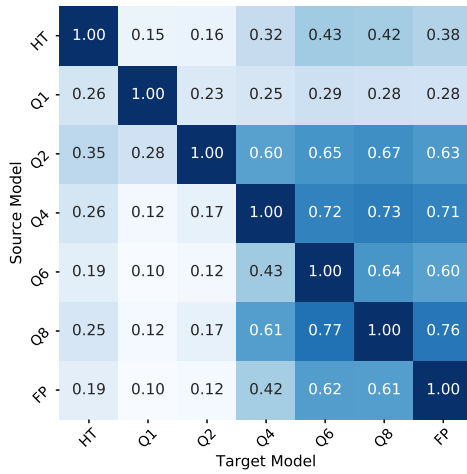


(a) Activation quantized VGG11 models

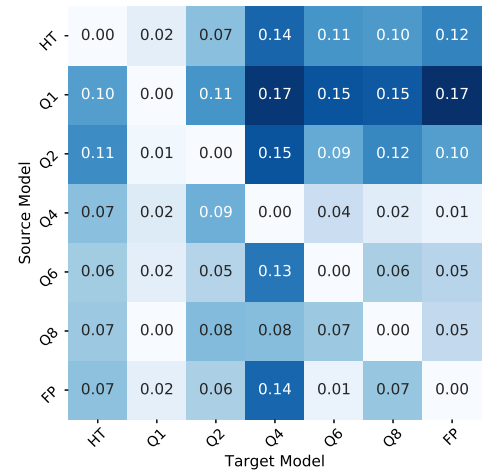


(b) Weight quantized VGG11 models

Fig. 11: Number of adversarial images transferred from source to target on CIFAR-10 dataset

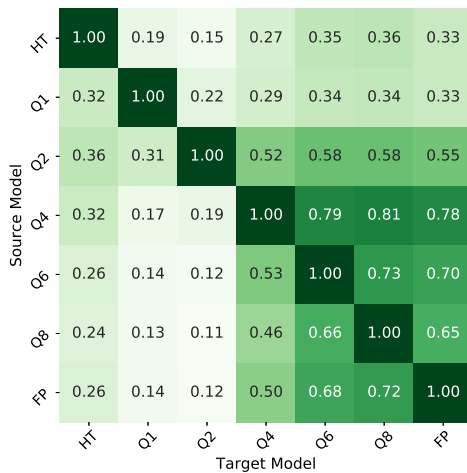


(a) CIFAR-10

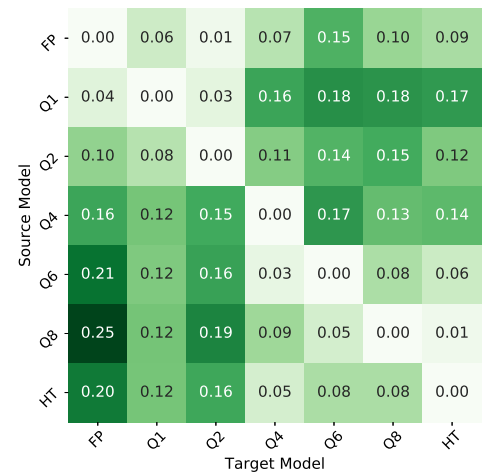


(b) CIFAR-10

Fig. 12: Actual TM and error in predictions for TM of quantized ResNet18 models at epsilon of 8/255 for CIFAR-10 dataset

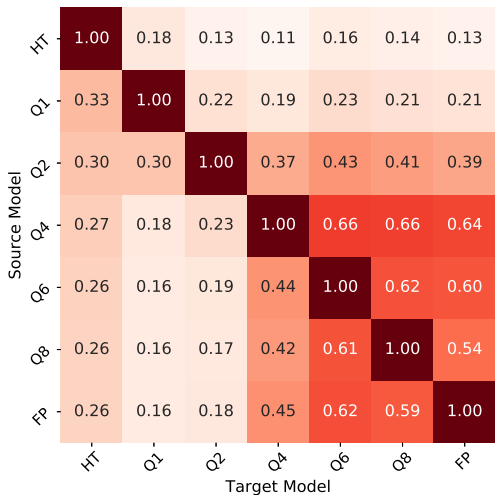


(a) CIFAR-100

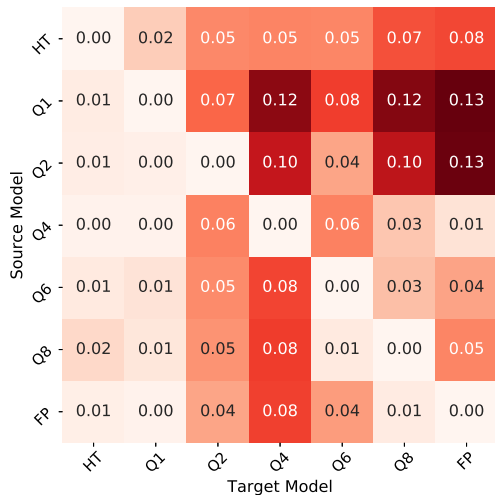


(b) CIFAR-100

Fig. 13: Actual TM and error in predictions for TM of quantized ResNet18 models at epsilon of 8/255 for CIFAR-100 dataset

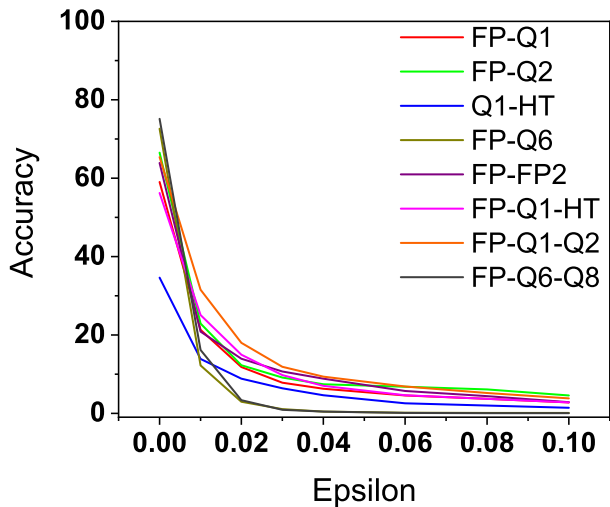


(a) Actual TM

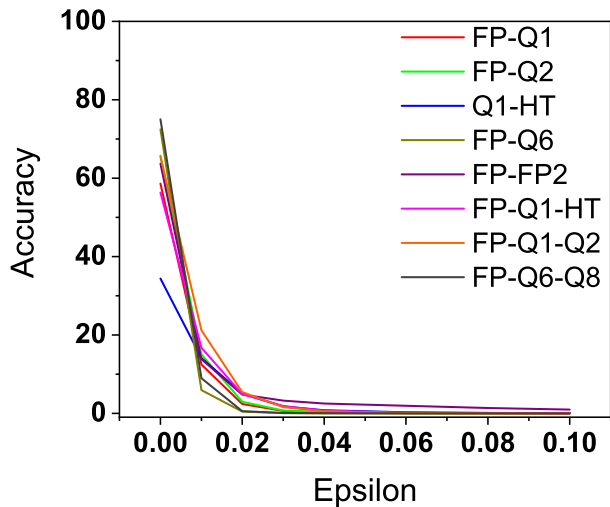


(b) Error in Prediction

Fig. 14: Actual TM and error in predictions for TM of quantized ResNet18 models at epsilon of 8/255 for ImageNet dataset



(a) CIFAR-100 Gradient Average



(b) CIFAR-100 Sign All

Fig. 15: Results for ensembles under different attacks for CIFAR-100.